Accepted Manuscript

Title: Evaluation of Mercury Stabilization Mechanisms by Sulfurized Biochars Determined using X-ray Absorption Spectroscopy

Authors: Peng Liu, Carol J. Ptacek, Krista M.A. Elena, David W. Blowes, W. Douglas Gould, Y. Zou Finfrock, Alana O. Wang, Richard C. Landis

PII: S0304-3894(17)30951-2
DOI: https://doi.org/10.1016/j.jhazmat.2017.12.051
Reference: HAZMAT 19083

To appear in: *Journal of Hazardous Materials*

Received date: 12-6-2017
Revised date: 16-12-2017
Accepted date: 19-12-2017

Please cite this article as: Liu P, Ptacek CJ, Elena KMA, Blowes DW, Gould WD, Finfrock YZ, Wang AO, Landis RC, Evaluation of Mercury Stabilization Mechanisms by Sulfurized Biochars Determined using X-ray Absorption Spectroscopy, *Journal of Hazardous Materials* (2010), https://doi.org/10.1016/j.jhazmat.2017.12.051

Evaluation of Mercury Stabilization Mechanisms by Sulfurized Biochars Determined using X-ray Absorption Spectroscopy

Peng Liu[a,b], Carol J. Ptacek[*,b], Krista M.A. Elena[b], David W. Blowes[b], W. Douglas Gould[b], Y. Zou Finfrock[c, d], Alana O. Wang[b], Richard C. Landis[e]

[a] School of Environmental Studies, China University of Geosciences, 388 Lumo Rd., Wuhan, Hubei, 430074, P. R. China
[b] Department of Earth and Environmental Sciences, University of Waterloo, 200 University Ave. W., Waterloo, ON, Canada N2L 3G1
[c] Science Division, Canadian Light Source Inc., 44 Innovation Boulevard, Saskatoon, SK, Canada S7N 2V3
[d] CLS@APS sector 20, Advanced Photon Source, Argonne National Laboratory, 9700 S. Cass Avenue, Argonne, IL 60439
[e] Formerly at E. I. du Pont de Nemours and Company, 974 Centre Road, Wilmington, DE 19805

[*] Corresponding author: Department of Earth and Environmental Sciences, University of Waterloo, 200 University Ave. W., Waterloo, ON, Canada N2L 3G1. Tel: +01 (519) 888 4567, 32230
E-mail: ptacek@uwaterloo.ca

GRAPHICAL ABSTRACT

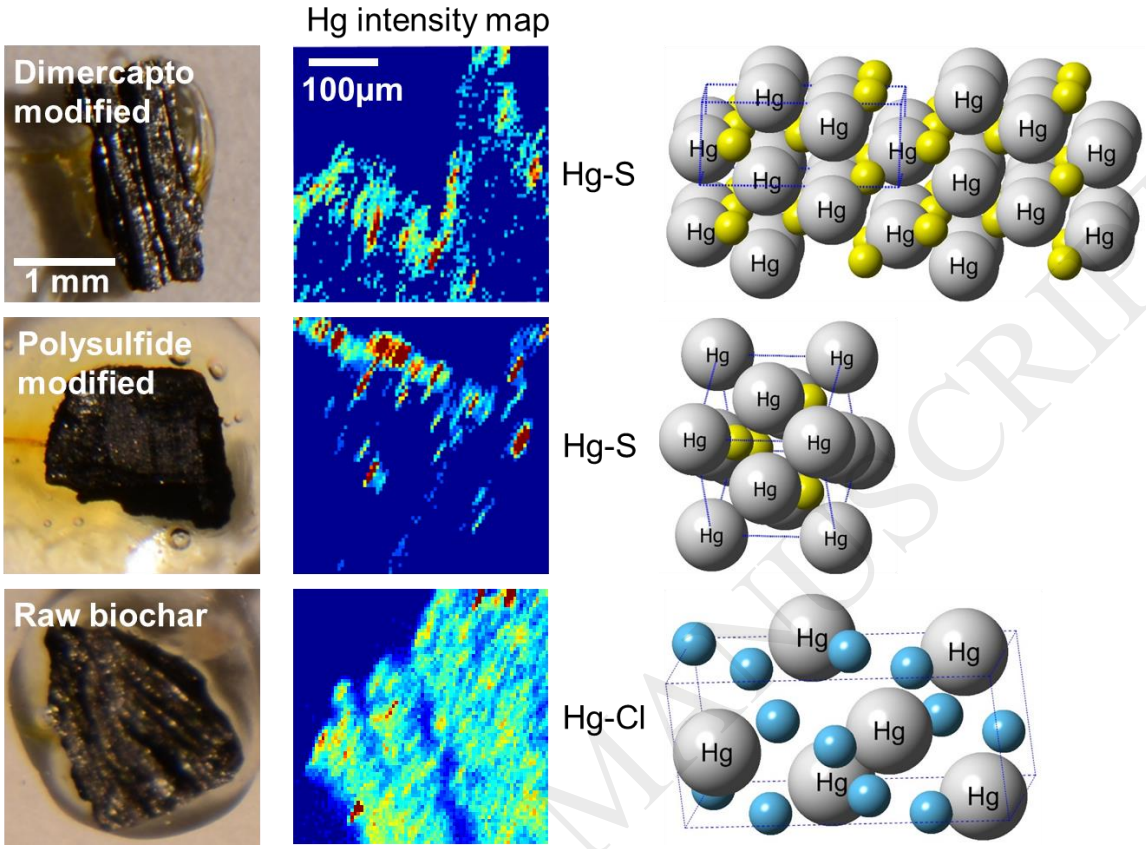

HIGHLIGHTS

- Hg removal was greatly improved by biochars after sulfurization
- Synchrotron-based techniques are utilized to characterize Hg removal mechanisms
- Polysulfur was chemisorbed and dimercato was sorbed by π-π interaction with biochar
- Hg distributes across the particle of unmodified biochar by bonding to Cl
- Hg distributes primarily on particle surface of sulfurized biochar by bonding to S

Abstract

The application of biochar to treat mercury (Hg) in the environment is being proposed on an increasing basis due to its widespread availability and cost effectiveness. However, the efficiency

of Hg removal by biochars is variable due to differences in source material composition. In this study, a series of batch tests were conducted to evaluate the effectiveness of sulfurized biochars (calcium polysulfide and a dimercapto-related compound, respectively) for Hg removal; Hg-loaded biochars were then characterized using synchrotron-based techniques. Concentrations of Hg decreased by >99.5% in solutions containing the sulfurized biochars. Sulfur X-ray absorption near-edge structure (XANES) analyses indicate a polysulfur-like structure in polysulfide-sulfurized biochar and a thiol-like structure (shifted compared to dimercapto) in the dimercapto-sulfurized biochar. Micro-X-ray fluorescence (μ-XRF) mapping and confocal X-ray micro-fluorescence imaging (CXMFI) analyses indicate Hg is distributed primarily on the edges of sulfurized biochar and throughout unmodified biochar particles. Hg extended X-ray absorption fine structure (EXAFS) analyses show Hg in enriched areas is bound to chlorine (Cl) in the unmodified biochar and to S in sulfurized biochars. These results indicate that Hg removal efficiency is enhanced after sulfurization through the formation of strong bonds (Hg-S) with S-functional groups in the sulfurized biochars.

Key words: Biochar; Mercury; Polysulfur; X-ray Absorption Spectroscopy; Confocal X-ray Micro-fluorescence Imaging

Introduction

Mercury (Hg) is a global high-priority contaminant in water, sediments, and soils [1]. Extensive efforts have been devoted to removing Hg from water and to stabilize Hg in soils, sediments, and solid-wastes to decrease its impact on the environment [2, 3]. Pyrolyzed carbonaceous materials, including activated carbon, charcoal, and biochar, have been used as reactive media in a variety of Hg treatment systems [4-9]. For example, Hg removal from aqueous solution using biochar derived from malt spent rootlets [10] and activated carbons derived from sago waste [11] and coirpith [12] have been shown to be effective; however, aqueous Hg concentrations after

treatment often remain in the μg L^{-1} to mg L^{-1} range, above those required for protection of the environment [13]. To overcome these limitations, functionalized resins have been used to achieve final aqueous concentrations of Hg in the ng L^{-1} range [14-18]. Synthetic chelating ligands have also been used to maximize Hg removal [19, 20]. These specialized resins and ligands can be costly, potentially limiting their use for large-scale Hg treatment as would be required for remediation of watershed-scale contamination. There remains a need to evaluate the effectiveness of low-cost reactive materials that promote removal of Hg to ng L^{-1} levels.

The bond between Hg(II) and sulfide or thiol compounds is strong [19-24], and has been extensively studied. Hg(II) is preferentially bonded to thiol functional groups compared to O/N ligands in organic mater [25-27]; Hg is likely complexed with two thiols in organic matter at a distance of 2.33 Å as indicated by Hg extended X-ray absorption fine structure (EXAFS) modeling. The binding with sulfide or thiol can result in a decrease in Hg bioavailability [28]. However, in some cases, the presence of polysulfide and low molecular weight-thiols in solution can lead to enhanced solubility of cinnabar and a potential increase in Hg bioavailability [29, 30]. Impregnation of polysulfide into carbonaceous materials can potentially reduce this adverse effect.

Calcium polysulfide (CPS) has been shown to be an effective reagent for removing Cr(VI) from water in both laboratory and field scale applications [31-33], and dimercapto (DMC)-related compounds have been studied for Hg removal with efficient removal of Hg observed [21, 34, 35]. Elemental S and H_2S have also been applied for activated carbon (AC) sulfurization [22, 23], but the process requires high temperatures and the H_2S gas is corrosive and toxic.

Characterization of the form and spatial distribution of Hg within biochar particles is important for understanding Hg removal mechanisms and estimating the stability of bonded Hg. Synchrotron-based techniques can be used to characterize Hg speciation and S species of the sulfurized sorbent, for example to observe Hg-Br, Hg-S, and Hg-C binding environments on brominated and sulfurized sorbents [22]. Feng et al. [23] report that elemental S, thiophene, and sulfate are likely responsible for Hg uptake in S-treated AC based on the results of S X-ray absorption near-edge structure (XANES) analyses.

Micro-X-ray fluorescence (μ-XRF) mapping has also been widely used to characterize the spatial distribution of Hg in various materials [36-40]. One drawback of μ-XRF mapping is that the fluorescence received by the detector is the sum of the signal along the incident beam path through the sample. Micro-XRF is often used to characterize elemental distributions in thin-sections, therefore measured distributions are representative of the sum of the elements over the thickness of a thin-section (usually ≥30 μm [8, 38, 40]). Confocal X-ray micro-fluorescence imaging (CXMFI), an emerging non-destructive technique, can overcome this drawback [41]. Depth compositional information can be obtained from precise locations of a particle using CXMFI [42]. The particle orientation can be adjusted using CXMFI, but for thin-sections, the slice of the particle is fixed.

In a previous study, Liu et al. [8] evaluated hardwood- (sp. *Quercus*) based biochar in its unmodified form and observed relatively effective removal of Hg from water. The current study is focused on improving Hg uptake by sulfurizing this biochar using CPS and DMC. A series of batch tests was conducted to evaluate the removal of dissolved Hg from aqueous solution using these sulfurized biochars. Solid-phase reaction products were examined using a range of

synchrotron-based techniques, including S K-edge XANES, μ-XRF, CXMFI, and Hg EXAFS analyses, to evaluate the forms and distribution of Hg within the sulfurized biochar particles.

Materials and Methods

Biochar Sulfurization

Biochar (CL2) was produced from oak wood at ~700°C (Cowboy Charcoal Co.). CPS (Green Earth Sure-Gro IP Inc.) and DMC (2,5-dimercapto-1,3,4-thiadiazole; 98%, Sigma-Aldrich) were used as biochar sulfurization reagents.

The biochar sulfurization was conducted under low-O_2 conditions. CL2 was crushed and sieved to a size of 0.5-2 mm and rinsed six times with Ar-purged ultra-pure water to remove fine particulates. The targeted S contents for the CL2 were 0.5, 2, and 5%. To achieve this, CL2 (20 g) was mixed with CPS (0.43, 1.7, and 4.2 mL) in 400 mL ultra-pure water or DMC (0.16, 0.63, and 1.56 g) in 100 mL ethanol. The mixtures were shaken thoroughly and allowed to equilibrate for 72 h. Controls were prepared by mixing CL2 with ultra-pure water. The supernatants were then decanted and the reactive materials were rinsed six times with ultra-pure water. The reactive materials were left to dry in the anaerobic chamber.

Batch Experiments

Batch-style experiments were conducted under low-O_2 conditions. Solutions containing 25 and 250 μg L^{-1} Hg were prepared in an anaerobic chamber by dissolving reagent-grade $HgCl_2$ in simulated groundwater (SG; $CaCO_3$-saturated water [43]). Duplicate tests were conducted in 40 mL polypropylene tubes by mixing 1 g reactive material with 40 mL Hg-spiked SG. SG with and without Hg as well as ultra-purified water were used as controls. The 40 mL tubes were rotated for 48 h. Samples were then collected for total Hg (THg) analysis by filtering through 0.45 μm membranes (Acrodisc®, Pall Corp.). Samples were acidified to pH<2 with concentrated HNO_3, and stored at 4°C until analysis.

The biochars without sulfurization and with 2% targeted S content were further tested in the same manner for removal of Hg at a higher initial concentration of Hg and for analysis with synchrotron-based techniques. The experiment was conducted by mixing 1 g of biochar with 200 mL SG with a THg concentration of 5 mg L^{-1}. Filtered samples were collected for THg and alkalinity analysis. Unfiltered samples were collected for pH analysis. Alkalinity and pH were measured immediately after sample collection. The pH was measured using an electrode (Orion-815600, Thermo Scientific). Alkalinity was determined in duplicate using a Hach® digital titrator, bromocresol green-methyl red indicator, and 0.16 N H_2SO_4.

THg concentrations were determined using cold-vapor atomic fluorescence spectroscopy (Tekran 2600) according to EPA Method1631 [44]. The method detection limit (MDL) was 0.19 ng L^{-1} as determined following an EPA procedure [45].

Solid Samples for X-Ray Absorption Spectroscopy

S reference materials included elemental S, Na_2SO_3 (Sigma-Aldrich), CPS, and DMC. Cinnabar (Excalibur Mineral Corp., Peekskill) was used as an Hg reference material. The reference materials were ground into fine powders to decrease self-absorption effects. Unmodified and sulfurized biochar samples with and without Hg were washed, freeze-dried, and ground into fine powders. The biochar samples loaded with Hg were prepared for thin-sections with a thickness of 30 μm (Vancouver Petrographics Ltd., Canada).

S X-Ray Absorption Near-Edge Structure Spectra

S K-edge XANES spectra were collected on the SXRMB beamline at the Canadian Light Source (CLS). Finely-ground samples and reference compounds were spread as a thin film on a conductive double-sided tape mounted to a copper sample holder. The reduction of higher-order harmonics was accomplished by detuning a Si(111) monochromator to 70%. An unfocused beam

of ~200×50 μm was employed and data were collected using a silicon drift detector. Both total electron (TEY) and fluorescence (FY) yield data were collected. TEY data were used for reference materials and sulfurized biochars because FY data are known to be susceptible to self-absorption at high S contents. FY data were collected for the unmodified biochars. Up to six scans were collected for each sample. Data was processed with ATHENA software [46]. The energy for each run was calibrated with elemental S. Spectra for $HgSO_4$, metacinnabar (β-HgS), cinnabar (α-HgS), pyrrhotite, pyrite, and L-cysteine were obtained from a previous study [8].

Micro-X-Ray Fluorescence Mapping

Micro-XRF maps were collected for thin-sections on Beamline 13-ID-E (GSECARS) at the Advanced Photon Source (APS), Argonne National Laboratory. A micro-focused beam with a size of ~2×2 μm^2 and a photon energy of 12.6 keV were applied. The step size (pixel) was 2×2 μm for the maps. A Vortex ME4 silicon drift diode array detector was placed at 90° relative to the incident beam to collect emitted XRF.

Confocal X-Ray Micro-Fluorescence Imaging

CXMFI analysis of the particles loaded with Hg was conducted at Beamline 20-ID-B (PNC/XSD), APS using an incident beam energy of 12.6 keV. The micro-focused beam size was ~2*2 μm^2. Particles were mounted on a quartz slide and placed at 35° to the incident beam. The XRF spectra were collected by a Si-drift Vortex detector perpendicular to the incident beam. A Ge optical unit (lithographically fabricated spoked channel array) was mounted in front of the detector to complete the confocal geometry [47-49].

The intensity attenuation was calculated for the incident beam and the XRF arising from the additional depth into the sample using the method described by Liu et al. [50]. The intensity was corrected using the Beer-Lambert Law by considering the heterogeneity of the sample. The

elemental composition used for correction is presented in Table S1. Data importing, processing, and plotting were completed in MATLAB®.

Hg Extended X-Ray Absorption Fine Structure Spectra

Hg EXAFS spectra were collected for the Hg-enriched areas of thin-sections on the GSECARS beamline at the APS. A short collection time (~5 min) was utilized to minimize the risk of beam damage. Five to ten scans were collected for each Hg-enriched area at 3 μm increments apart between each scan to reduce radiation exposure (beam size: ~2×2 μm). The scans were merged for further data processing.

The XAS spectra were analyzed using ATHENA, and EXAFS model calculations were made using ARTEMIS [46] following the method described by Gibson et al. [35] and Liu et al. [8]. The atomic structures of cinnabar, metacinnabar, $HgCl_2$, Hg_2Cl_2, and HgO from American Mineralogist Crystal Structure database [51] and ATOMS.INP website [52], were used as models for fitting of sample EXAFS spectra. The atomic structure of Hg(II) complexed with two thiols ($Hg(SR)_2$) were also constructed from Skyllberg et al. [25], and was used as a model structure. The EXAFS spectra were modelled using the first shell of these reference materials, and were fitted in Fourier-transformed R-space.

During the refinement of the first shell of Hg bound to biochar, the amplitude reduction factor (S_0^2) and the Debye-Waller factor (σ^2) were fixed on values determined from fits to reference compounds [8], and the coordination number (*CN*) and bond distances (*R*) of the first shell were varied. A *k* weighting of 3 was applied to enhance weak oscillations in the EXAFS spectra. The best fitted results were reported by evaluating the values of *CN* (*CN*>0), the change in interatomic distance (ΔR), the change in energy from theoretical data (ΔE; abs(ΔE)<10 eV), and goodness of fit (R-factor).

Results and Discussion

Aqueous Chemistry

Batch experiment pH values increased slightly after the addition of unmodified and sulfurized biochars. The initial pH values were 7.9, 7.6, and 7.3 in solutions with THg concentrations of 17,800 ng L^{-1}, 245,000 ng L^{-1}, and 4,960 µg L^{-1}, respectively. At the termination of the experiment, the pH values increased to ~8.2 in all solutions mixed with washed and unmodified hardwood-based biochar (CL2), CPS-sulfurized CL2 (CL2-CPS), and DMC-sulfurized CL2 (CL2-DMC). The initial alkalinity was ~95 mg L^{-1}, which is close to the values at the termination of the experiment. The results indicate the aqueous chemistry of the solution was only slightly altered after the addition of washed CL2 and sulfurized CL2. This observation was not the case for the unwashed and unmodified hardwood-based biochar [53], for which the pH increased from 7.8 to 8.5 and the alkalinity increased from 44 to 74 mg L^{-1}.

Hg Removal

Substantial decreases in THg concentrations were observed for solutions with added CL2, CL2-CPS, and CL2-DMC at three different initial concentrations (Fig. 1). The final THg concentrations in solutions containing sulfurized CL2 were much lower than those with CL2. When the initial THg concentration was 17,800 ng L^{-1}, the average final THg concentration was 370 ng L^{-1} using CL2, but <40 ng L^{-1} using CL2-CPS or CL2-DMC. When the initial THg concentration was 245,000 ng L^{-1}, the final concentration was 5,700 ng L^{-1} using CL2 but <110 ng L^{-1} using the sulfurized CL2. When the initial THg concentration was 4,960 µg L^{-1}, the final concentration was 170 µg L^{-1} using CL2 but <28 µg L^{-1} using the sulfurized CL2. THg removal was >96.5 and >99.5% using CL2 and the sulfurized CL2, respectively, at the three initial concentrations.

The observed decline in Hg concentrations indicates that Hg removal is much more effective in the batch mixtures containing the sulfurized biochar particles. No clear trend in THg concentrations is observed with respect to the use of CL2-CPS at three targeted S contents (0.5, 2, and 5%), but, in contrast, THg concentrations decrease after addition of CL2-DMC when the targeted S content increases.

Hg is more effectively removed by CL2-DMC than CL2-CPS at a low initial THg concentration, but more effectively removed by CL2-CPS at high initial concentrations. The more effective Hg removal by CL2-DMC at the lowest THg concentration evaluated may be due to higher binding constants for Hg-thiol interaction than for Hg-polysulfide interaction [54]. The greater Hg removal by CL2-CPS at a high concentration may be due to a higher proportion of reaction sites provided by CL2-CPS compared to CL2-DMC.

The Hg removal efficiency observed using these sulfurized biochars is comparable to previous studies using functionalized resins and activated carbon. For example, Hg concentrations decrease from 1000 to <12 ng L^{-1} in batch experiments and to <51 ng L^{-1} in column experiments using functionalized resins [16, 17]; THg concentrations decrease from approximately 10,000 to 25 ng L^{-1} in batch experiments using activated carbon [8].

S XANES

S XANES spectra can be used to define the oxidation state of S based on the position of the characteristic peak. The peak energy of S standards increases from 2470.3 to 2482.5 eV when the oxidation state of S increases from -2 (sulfide) to +6 (sulfate) (Fig. 2). The peaks in the S XANES spectra assigned to ν1-5 represent the major peaks observed in CPS, DMC, CL2, DMC-CL2, and CPS-CL2 (Fig. 2). Three peaks (ν1, 2471.1; ν2, 2472.8; ν4, 2478.2 eV) are observed for CPS (Fig. 2a). The ν1 peak falls between peaks in the spectra of FeS_2 and FeS, and is due to

the excitation of 1*s* electrons from the end members of S in the polysulfide. The ν2 peak is at the same position as the peak in elemental S, and is assigned to 1*s* electrons in a molecular orbital σ^* (S-S) of the intermediate members of polysulfide. The ν4 peak is close to that of sulfite, and another small peak is observed at a higher energy and may represent an impurity in CPS. ν3 (2473.6 eV) in DMC, at the same position as the peak in L-cysteine, is assigned to a $1s \rightarrow \sigma^*$ transition (S-C and S-H) [55, 56]. The pre-edge small peak (2471.21 eV) in DMC is likely due to the excitation of electrons from the S between the two carbon atoms of DMC.

The two peaks at low energy and the ν5 peak (sulfate, 2482.6 eV) in CL2 are not distinguishable after sulfurization to CL2-CPS and CL2-DMC (Fig. 2b), which is likely due to the low S content (<0.01%) in CL2 [8]. Only the ν2 peak is observed in CL2-CPS, which indicates that the elemental S-like structure (polysulfur) is primarily formed during the sulfurization process. This observation also indicates that the impurities in CPS are removed during the washing process. For CL2-DMC, a shoulder at the same energy as ν2 is observed on the $\nu3^+$ peak. This shoulder is likely due to the shift of the pre-edge small peak in DMC. The $\nu3^+$ means the peak is at a slightly higher energy (2474.1 eV) than ν3. The slight shifts of ν3 to $\nu3^+$ and the pre-edge small peak are likely due to the interaction of thiol groups on DMC and functional groups on CL2. The observation of the polysulfur structure in CL2-CPS is consistent with spectra reported for activated carbon fibers treated with H_2S at 400-600°C [23].

The disappearance of the ν1 peak representing the end members of the polysulfide in the S spectra for CL2-CPS indicates the end members are likely embedded into the carbon structure of the biochar. The impregnation of CPS in CL2 is likely through a chemisorption process (Eq. 1). Aromatic ring structures of biochar have been reported [57, 58], and these aromatic ring structures have delocalized electrons (π electrons). The thiadiazole in DMC also has delocalized

electrons [59, 60]. Therefore, DMC is likely bound to biochar via π-π interactions between the ring structures (Eq. 2). The π-π interactions between biochar and DMC cannot alter the S speciation in DMC, which is consistent with the similarity of the S spectra between DMC and CL2-DMC. This type of interaction is hydrophobic and provides thiol groups that are available to bind with Hg.

$$2\text{-C} + S_x^{2-} = \text{-C-}S_x\text{-C-}, \quad (1)$$

$$\text{-C}\pi + \pi\text{DMC} = \text{-C}\pi\text{- }\pi\text{DMC}. \quad (2)$$

where -C represents the end member of a C chain, S_x^{2-} represents polysulfur, and -Cπ represents delocalized electrons of aromatic rings [61].

The sulfurized biochars were exposed to air for 10 and 60 d to evaluate the stability of the deposited S. The spectra collected for CL2-CPS exposed to air for 10 or 60 d are similar to those for the fresh materials (Fig. 2c). The result indicates S in CL2-CPS is stable under aerobic conditions. A sulfate peak is evident in CL2-DMC exposed to air for 60 d, which indicates S in CL2-DMC is not as stable as S in CL2-CPS.

The form of S in reactive materials (*e.g.*, elemental, cysteine, and thiophene) plays an important role in the Hg removal process [23, 40, 62]. The S XANES spectra of CL2-CPS loaded with Hg are similar to CL2-CPS without Hg (Fig. 2b). This observation indicates the S forms in CL2-CPS are not altered by the adsorption of Hg, similar to previous findings by Liu et al. [8] for unmodified CL2 with and without Hg exposure. The peak height is slightly different for CL2-DMC without and with Hg, and a sulfate peak is evident in CL2-DMC loaded with Hg.

Hg μ-XRF Maps

The results of μ-XRF maps indicate differences in the Hg distribution in thin-sections prepared using CL2, CL2-CPS, and CL2-DMC particles loaded with Hg (Fig. 3). For CL2, Hg is located

inside the pores and channels within the particles. For CL2-CPS, Hg is primarily distributed on the surface with less observed within the pores of the particles. For CL2-DMC, Hg is mostly located on the surface of and also penetrates less extensively into the particles. The presence of Hg is confirmed in the XRF spectra collected from an Hg-enriched area (Fig. 3).

The difference in Hg distribution patterns between unmodified (CL2) and sulfurized (CL2-DMC and CL2-CPS) biochars is likely due to impregnation of S in the sulfurized biochars. The primary distribution of Hg on the surface of sulfurized biochars indicates the S likely bonded to the surface, which is consistent with a previous study that reported Hg concentrated on the exterior of a polysulfide-rubber-coated activated carbon, but diffused up to 100 μm into the particle after 3 months [38]. Results from this study indicate the Hg is distributed up to 10 μm into the sulfurized biochar particles after 2 d of treatment. The Hg distribution within the channel-like shape in CL2 is consistent with the observation of another thin-section of the same biochar in a previous study [8].

Confocal X-Ray Micro-Fluorescence Imaging

Large differences in Hg distribution are evident for unmodified and sulfurized biochars based on CXMFI analysis (Fig. 4). Hg is distributed across and deep into CL2 particles but mostly accumulates on the surface of CL2-CPS particles. Hg penetrates slightly deeper into CL2-DMC than CL2-CPS. Additional CXMFI results for Hg distribution within unmodified and sulfurized biochar particles are provided in Figs. S1-S5; distribution maps of other elements (S, Cl, K, and Ca) are also presented. Consistent Hg distribution maps are observed for the particles presented in Fig. 4 and in Figs. S1-S5. The observations are also consistent with the μ-XRF maps (Fig. 3).

The S intensity of unmodified biochar particles in the maps is indistinguishable from the background signal and therefore is not included. The distribution of S is primarily on the surface

of CL2-CPS (Figs. S2-S4) and on the surface and along the pores of CL2-DMC (Fig. S5). The observation of S in the sulfurized biochars indicates that it was successfully incorporated into the biochars. The Hg in enriched areas co-occurs with S in the sulfurized biochars (Fig. S2-S5). The difference in Hg distribution between the sulfurized biochars is likely due to the difference in S distribution.

Hg EXAFS

The threshold E_0 (ionization energy) is 12.285 keV for the Hg XANES spectra of Hg-enriched areas of the unmodified and sulfurized biochars (Fig. 5). No distinguishable features are observed among the XANES spectra of the samples. The Hg XANES spectra of the samples indicate Hg is in the oxidized Hg(II) form, as indicated by the similarity of the E_0 and edge shape of the sample spectra and the spectra for HgO, $HgCl_2$, cinnabar, and metacinnabar [8, 50].

Modeling EXAFS spectra can help to define the local structural information (*e.g.*, binding elements, coordination number, bond length) of the atom of interest. The best matches are obtained using $HgCl_2$ as a model compound to simulate the spectra for Hg-enriched areas of unmodified CL2 (Table 1). The spectra for Hg-enriched areas of CL2-CPS and CL2-DMC were best simulated by using the structure of cinnabar(Table 1). The Hg EXAFS modeling results indicate that Hg is bound to Cl in the unmodified biochar and to S in the sulfurized biochar. The EXAFS modeling R-factors range from 0.08 to 0.12.

The coordination number (*CN*) of Cl is 0.6 for Hg in the Hg-enriched area of CL2, a value that is close to previous measurements using the same biochar [8]; the bond length is 2.29 Å, which is consistent with the theoretical value for Hg-Cl bonding. The *CNs* of S bound to Hg are 1.3 and 1.7 in Hg-enriched areas of CL2-CPS and CL2-DMC, which are in the range of published values [8, 35, 63]; the modeled Hg-S distances are 2.36 and 2.42 Å, which are similar

to the theoretical value for cinnabar (2.37 Å) [8]. Gibson et al. [35] conducted a batch experiment using DMC to remove Hg from solution and bulk Hg EXAFS was modeled with the first path of cinnabar. The results show *CN* is 1.6 and bond length is 2.48 Å [35], which are similar to the current study using CL2-DMC.

The Hg EXAFS modelling results indicate HgS is the primary Hg species in Hg-enriched areas of sulfurized biochars, suggesting that a chemical reaction occurs between the Hg in solution and the S functional groups in the biochars. Kim et al. [38] also report Hg removal through reaction with S in polysulfide-rubber-coated activated carbon. Based on the EXAFS modeling results, the following reactions are summarized to describe Hg removal pathways using CL2 (Eq. 3), CL2-CPS (Eq. 4), and CL2-DMC (Eq. 5).

$$2\text{-Cl} + Hg(OH)_2^0 + 2H^+ \rightarrow \text{-Cl-Hg-Cl-} + 2H_2O, \quad (3)$$

$$\text{-S-S-} + Hg(OH)_2^0 + 2H^+ \rightarrow \text{-S(Hg)S-} + 2H_2O, \quad (4)$$

$$2\text{-SH} + Hg(OH)_2^0 = \text{-S-Hg-S-} + + 2H_2O. \quad (5)$$

where -Cl is chlorine from the biochar matrix or from solution, -S-S- is chemisorbed polysulfur of CPS, and -SH is thiol from adsorbed DMC. $Hg(OH)_2^0$ is the primary Hg species at the pH range (7.3-8) of the initial solution [64, 65].

Conclusions

Hg immobilization by reaction or complexation with S functional groups within sulfurized biochar is a potential strategy for remediating contaminated sites by limiting Hg transport and decreasing Hg bioavailability. Results of this study indicate that Hg removal is enhanced after sulfurization of an oak biochar compared with unmodified biochar. After treatment, the Hg is distributed mainly on the surface of sulfurized biochars and on the surface and within the unmodified biochar particles. Synchrotron-based analyses indicate that Hg is stabilized through formation of Hg-S for the sulfurized biochar, suggesting a potentially stronger binding

mechanism relative to simple surface adsorption processes. Future research is still required to evaluate the stability of Hg removed by the sulfurized biochars under long-term and other conditions, including redox oscillation, acidic or basic conditions.

Contaminated-site remediation using DMC or DMC-sulfurized reactive materials has not been reported, however, DMC-sulfurized material has been used in the removal of metal ions from ethanol [66]. DMC has also been used for determinations of Hg, and Cu in different environmental media, due to its propensity to bind with metals [67]. A potential application of CL2-DMC for Hg removal is in controlled environments such as use in containerized treatment systems for wastewater [68]. Larger-scale field applications may require greater information on the potential health effects of DMC.

CPS is a low-cost (~\$0.32 L^{-1} [69]) reagent approved for use for contaminated site remediation (including Superfund sites) in the US [70]. After impregnation of CPS in the biochar, stabilization of Hg is enhanced, potentially decreasing the environmental impact of Hg. Biochar can be stable under some environmental settings for long periods [71], suggesting that sulfurized biochar may also be stable over the long term.

Acknowledgements

This research was funded by the Natural Sciences and Engineering Research Council of Canada (NSERC), E. I. du Pont de Nemours and Company, and the Canada Research Chair program. Synchrotron-based techniques were performed at GSECARS and PNC/XSD (CLS@APS) of APS, at SXRMB, CLS. This research was performed using optics provided by Cornell High Energy Synchrotron Source. The CLS is supported by the Canada Foundation for Innovation, NSERC, the University of Saskatchewan, and others. Peng Liu received travel support from the CLS. We appreciate advice and assistance received from the South River Science Team and D.

Peak, E.E. Mack, J. Dyer, N. Grosso, M. Newville, T. Lanzirotti, R. Gordon, Y. Hu, J. Ma, and Y.Y. Liu.

Table 1. Hg EXAFS fitting results for Hg-enriched areas of thin-sections[a].

Sample	Reference	Path	CN	R (Å)	S_0^2	σ^2 (Å^2)	R-factor
CL2-DMC	α-HgS	Hg-S	1.3 (±0.3)	2.36 (±0.04)	0.841[b]	0.00518[b]	0.12
CL2-CPS	α-HgS	Hg-S	1.7 (±0.7)	2.42 (±0.07)	0.841[b]	0.00518[b]	0.11
CL2	$HgCl_2$	Hg-Cl	0.6 (±0.2)	2.29 (±0.07)	0.967[b]	0.00234[b]	0.08

[a] CN = coordination number, R = bond length, and R-factor = fitting statistic

[b] fixed values from model compounds [8, 50]

The value in the bracket is error bar which is taken from the diagonal of a covariance matrix.

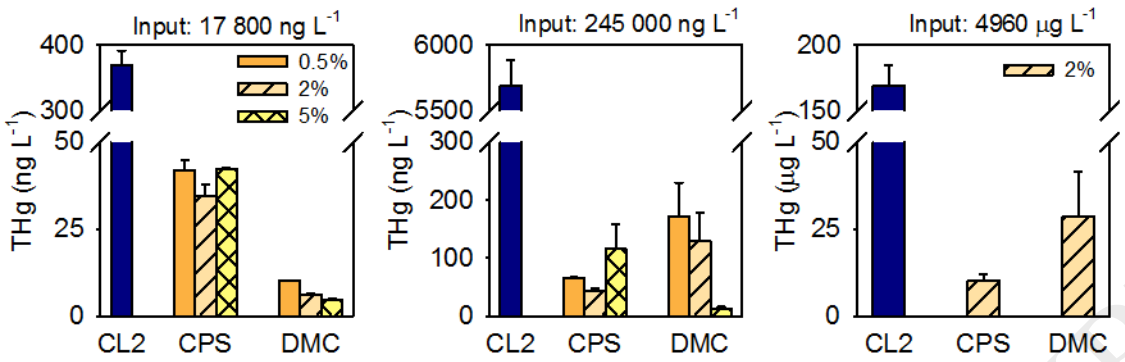

Figure 1. THg concentrations from aqueous solution in batch tests containing CL2, CL2-CPS and CL2-DMC (target S contents: 0.5, 2, and 5%) at three initial concentrations. Error bars represent standard error of the mean derived from duplicate experiments.

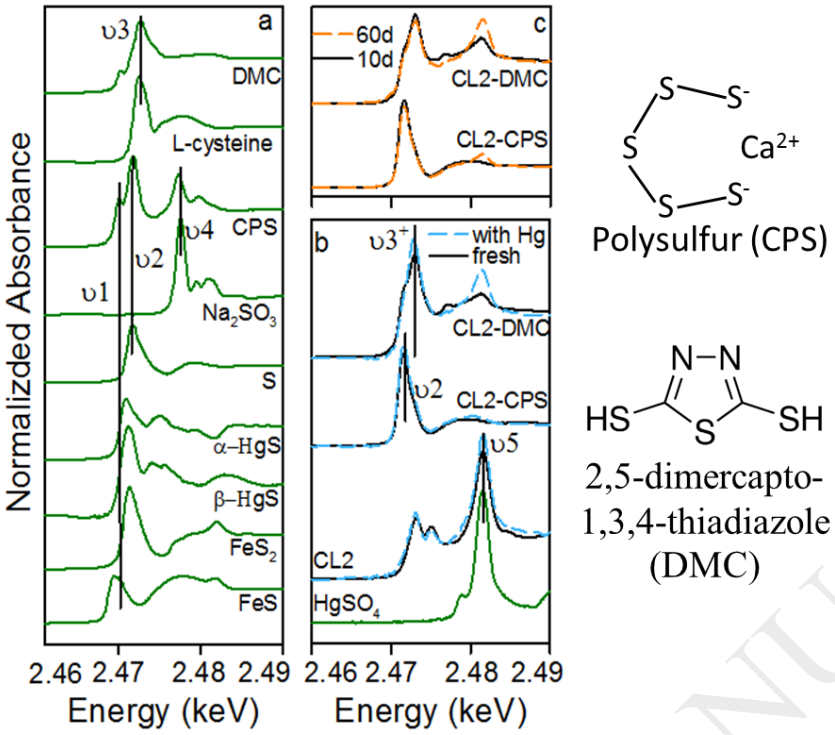

Figure 2. S XANES spectra of a) ten reference materials (one in b), b) unmodified and sulfurized CL2, and c) sulfurized CL2 exposed to air for 10 and 60 d. Spectra of S^0 and $HgSO_4$ were reduced by half for ease of display. The molecular structures of CPS and DMC are presented.

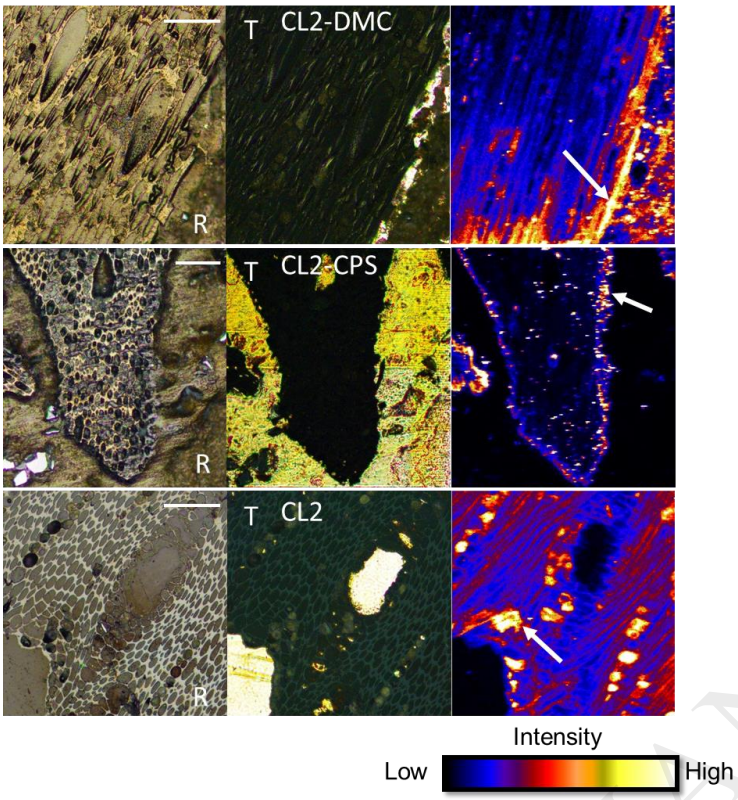

Figure 3. Microscope photos under reflection mode (left), transmission mode (medium), Hg μ-XRF maps (right). White bar represents 100 μm. EXAFS spectra for modeling were collected at locations indicated by white arrows.

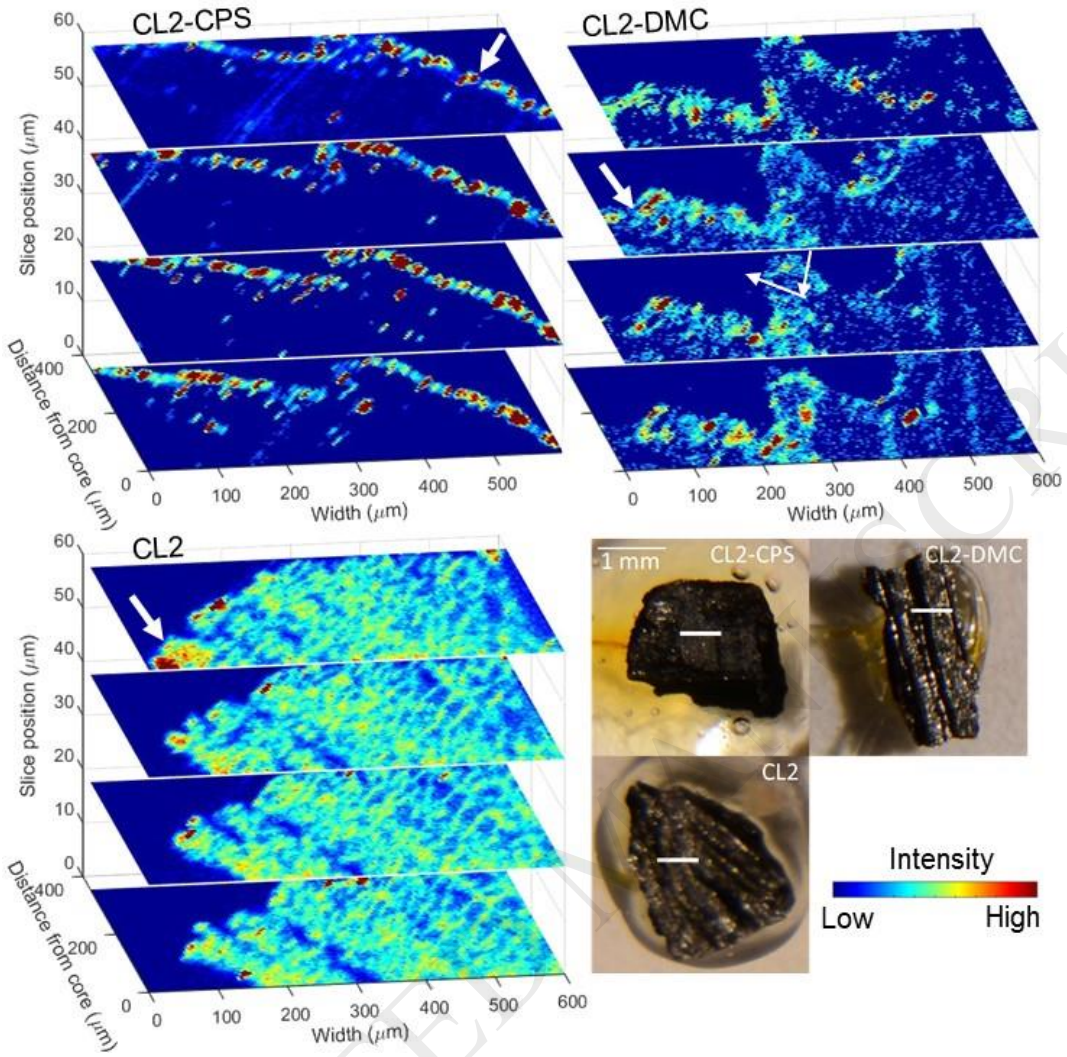

Figure 4. Confocal X-ray micro-fluorescence imaging showing the distribution of Hg in unmodified and sulfurized biochars with adsorbed Hg. Photos in the bottom right corner show the orientation of the particles for analysis. The white bars on the particle indicate the imaging area (600×60 μm^2) with an imaging depth as 350 μm. The thick white arrow indicates the surface of the particle. The thin white arrows indicate the incident and emitted beam paths.

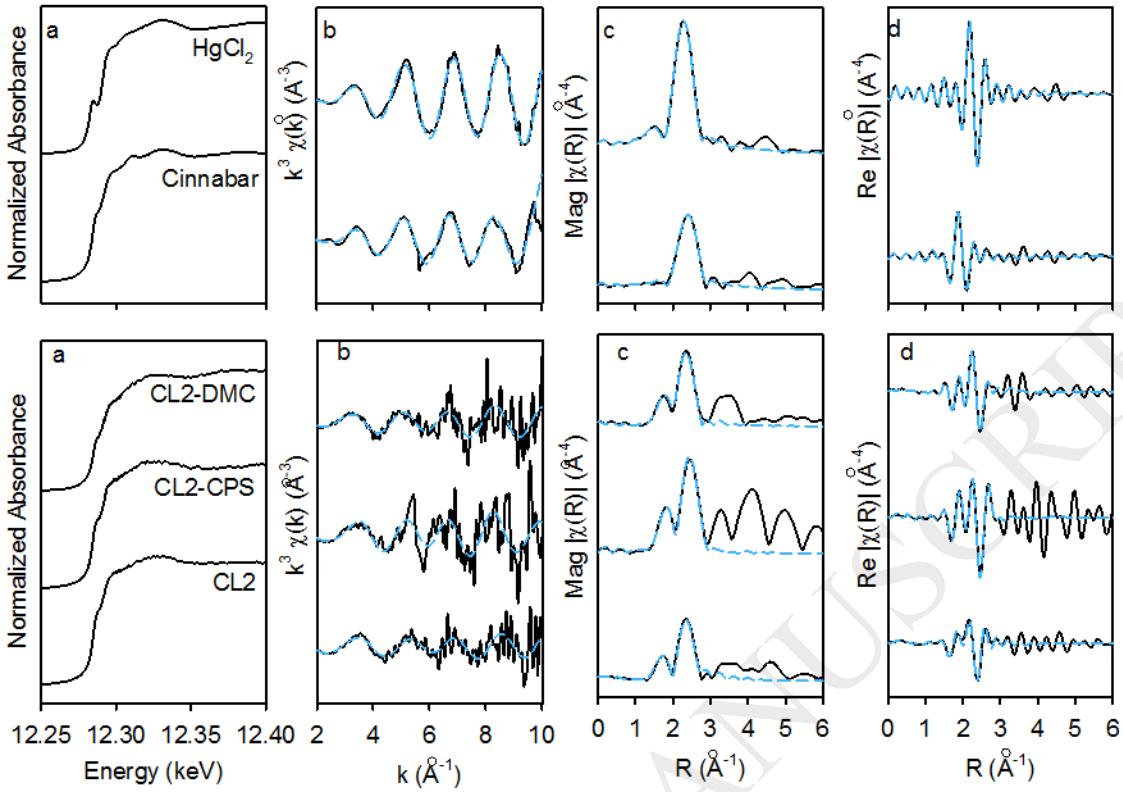

Figure 5. a) Normalized Hg XANES spectra of $HgCl_2$ and cinnabar, and spectra collected from Hg-enriched areas in thin-sections. b) k^3-weighted chi spectra (black line) and best fit (blue-dash line). c) Fourier-transformed magnitude spectra. d) Fourier-transformed real part.

Reference

[1] P.B. Tchounwou, W.K. Ayensu, N. Ninashvili, D. Sutton, Environmental exposure to mercury and its toxicopathologic implications for public health, Environ. Toxicol., 18 (2003) 149-175.

[2] P.M. Randall, S. Chattopadhyay, Mercury contaminated sediment sites-An evaluation of remedial options, Environ. Res., 125 (2013) 131-49.

[3] J. Wang, X. Feng, C.W.N. Anderson, Y. Xing, L. Shang, Remediation of mercury contaminated sites - A review, J. Hazard. Mater., 221-222 (2012) 1-18.

[4] D. Mohan, A. Sarswat, Y.S. Ok, C.U. Pittman Jr, Organic and inorganic contaminants removal from water with biochar, a renewable, low cost and sustainable adsorbent - A critical review, Bioresour. Technol., 160 (2014) 191-202.

[5] J.L. Gomez-Eyles, C. Yupanqui, B. Beckingham, G. Riedel, C. Gilmour, U. Ghosh, Evaluation of biochars and activated carbons for *in situ* remediation of sediments impacted with organics, mercury, and methylmercury, Environ. Sci. Technol., 47 (2013) 13721-13729.

[6] C.C. Gilmour, G.S. Riedel, G. Riedel, S. Kwon, R. Landis, S.S. Brown, C.A. Menzie, U. Ghosh, Activated carbon mitigates mercury and methylmercury bioavailability in contaminated sediments, Environ. Sci. Technol., 47 (2013) 13001-13010.

[7] C.R. Patmont, U. Ghosh, P. LaRosa, C.A. Menzie, R.G. Luthy, M.S. Greenberg, G. Cornelissen, E. Eek, J. Collins, J. Hull, T. Hjartland, E. Glaza, J. Bleiler, J. Quadrini, In situ sediment treatment using activated carbon: A demonstrated sediment cleanup technology, Integr. Environ. Assess. Manag., 11 (2015) 195-207.

[8] P. Liu, C.J. Ptacek, D.W. Blowes, R.C. Landis, Mechanisms of mercury removal by biochars produced from different feedstocks determined using X-ray absorption spectroscopy, J. Hazard. Mater., 308 (2016) 233-242.

[9] H. Li, X. Dong, E.B. da Silva, L.M. de Oliveira, Y. Chen, L.Q. Ma, Mechanisms of metal sorption by biochars: Biochar characteristics and modifications, Chemosphere, 178 (2017) 466-478.

[10] L.G. Boutsika, H.K. Karapanagioti, I.D. Manariotis, Aqueous mercury sorption by biochar from malt spent rootlets, Water Air Soil Poll., 225 (2014) 1-10.

[11] K. Kadirvelu, M. Kavipriya, C. Karthika, N. Vennilamani, S. Pattabhi, Mercury(II) adsorption by activated carbon made from sago waste, Carbon, 42 (2004) 745-752.

[12] C. Namasivayam, K. Kadirvelu, Uptake of mercury (II) from wastewater by activated carbon from an unwanted agricultural solid by-product: Coirpith, Carbon, 37 (1999) 79-84.

[13] S.M. Ullrich, T.W. Tanton, S.A. Abdrashitova, Mercury in the aquatic environment: A review of factors affecting methylation, Crit. Rev. Environ. Sci. Technol., 31 (2001) 241-293.

[14] K.T. Klasson, K. Kosny, S.R. Drescher, G.R. Southworth, J.F. Hensley, Reaching parts per trillion clean-up criterion for mercury in water, in: Waste Management 2003 Symposium, Tucson, AZ, 2003, pp. 23-27.

[15] K. Klasson, D. Bostick, L. Farr, D. McTaggart, P. Taylor, Demonstration of mercury sorbents to meet DOE customer needs (Report#: ORNL/TM-2000/12), Oak Ridge National Laboratory, TN, 2000.

[16] W. Hollerman, L. Holland, D. Ila, J. Hensley, G. Southworth, T. Klasson, P. Taylor, J. Johnston, R. Turner, Results from the low level mercury sorbent test at the Oak Ridge Y-12 Plant in Tennessee, J. Hazard. Mater., 68 (1999) 193-203.
[17] K.T. Klasson, D.T. Bostick, Trace-level mercury removal from surface water (Report#: ORNL/CP-98108), Oak Ridge National Laboratory, TN, 1998.
[18] D. Bostick, K. Klasson, Multi-weight isotherm results for mercury removal in upper East Fork Popular Creek water (Report#: ORNL/TM--13582), Oak Ridge National Laboratory, TN, 1998.
[19] L.Y. Blue, P. Jana, D.A. Atwood, Aqueous mercury precipitation with the synthetic dithiolate, BDTH2, Fuel, 89 (2010) 1326-1330.
[20] L.Y. Blue, M.A. Van Aelstyn, M. Matlock, D.A. Atwood, Low-level mercury removal from groundwater using a synthetic chelating ligand, Water Res., 42 (2008) 2025-2028.
[21] O. Olkhovyk, M. Jaroniec, Ordered mesoporous silicas with 2,5-dimercapto-1,3,4-thiadiazole ligand: High capacity adsorbents for mercury ions, Adsorption, 11 (2005) 205-214.
[22] T.M. Bisson, Z.Q. Ong, A. MacLennan, Y. Hu, Z. Xu, Impact of sulfur loading on brominated biomass ash on mercury capture, Energ. Fuel, 29 (2015) 8110-8117.
[23] W. Feng, E. Borguet, R.D. Vidic, Sulfurization of a carbon surface for vapor phase mercury removal - II: Sulfur forms and mercury uptake, Carbon, 44 (2006) 2998-3004.
[24] N. Asasian, T. Kaghazchi, Comparison of dimethyl disulfide and carbon disulfide in sulfurization of activated carbons for producing mercury adsorbents, Ind. Eng. Chem. Res., 51 (2012) 12046-12057.
[25] U. Skyllberg, P.R. Bloom, J. Qian, C.M. Lin, W.F. Bleam, Complexation of mercury(II) in soil organic matter: EXAFS evidence for linear two-coordination with reduced sulfur groups, Environ. Sci. Technol., 40 (2006) 4174-4180.
[26] K. Xia, U.L. Skyllberg, W.F. Bleam, P.R. Bloom, E.A. Nater, P.A. Helmke, X-ray absorption spectroscopic evidence for the complexation of Hg(II) by reduced sulfur in soil humic substances, Environ. Sci. Technol., 33 (1999) 257-261.
[27] D. Hesterberg, J.W. Chou, K.J. Hutchison, D.E. Sayers, Bonding of Hg(II) to reduced organic sulfur in humic acid as affected by S/Hg ratio, Environ. Sci. Technol., 35 (2001) 2741-2745.
[28] E.-A. Kim, A.L. Seyfferth, S. Fendorf, R.G. Luthy, Immobilization of Hg(II) in water with polysulfide-rubber (PSR) polymer-coated activated carbon, Water Res., 45 (2011) 453-460.
[29] J.A. Jay, F.M.M. Morel, H.F. Hemond, Mercury speciation in the presence of polysulfides, Environ. Sci. Technol., 34 (2000) 2196-2200.
[30] H. Hsu-Kim, K.H. Kucharzyk, T. Zhang, M.A. Deshusses, Mechanisms regulating mercury bioavailability for methylating microorganisms in the aquatic environment: A critical review, Environ. Sci. Technol., 47 (2013) 2441-56.
[31] M. Chrysochoou, C.P. Johnston, Polysulfide speciation and reactivity in chromate-contaminated soil, J. Hazard. Mater., 281 (2015) 87-94.
[32] R.J.F. Bewley, S. Clarke, Field application of calcium polysulphide for ex situ treatment of soils contaminated with chromite ore processing residue, Land Contam. Reclam., 18 (2010) 1-12.

[33] M. Chrysochoou, C.P. Johnston, G. Dahal, A comparative evaluation of hexavalent chromium treatment in contaminated soil by calcium polysulfide and green-tea nanoscale zero-valent iron, J. Hazard. Mater., 201-202 (2012) 33-42.
[34] O. Olkhovyk, M. Jaroniec, Adsorption characterization of ordered mesoporous silicas with mercury-specific immobilized ligands, Adsorption, 11 (2005) 685-690.
[35] B.D. Gibson, C.J. Ptacek, M.B.J. Lindsay, D.W. Blowes, Examining mechanisms of groundwater Hg(II) treatment by reactive materials: An EXAFS study, Environ. Sci. Technol., 45 (2011) 10415-21.
[36] S. Serrano, D. Vlassopoulos, P.A. O'Day, Mechanism of Hg(II) immobilization in sediments by sulfate-cement amendment, Appl. Geochem., 67 (2016) 68-80.
[37] B. Gu, B. Mishra, C. Miller, W. Wang, B. Lai, S.C. Brooks, K.M. Kemner, L. Liang, X-ray fluorescence mapping of mercury on suspended mineral particles and diatoms in a contaminated freshwater system, Biogeosciences Discuss., 11 (2014) 7521-7540.
[38] E.A. Kim, Y. Masue-Slowey, S. Fendorf, R.G. Luthy, Intra-particle migration of mercury in granular polysulfide-rubber-coated activated carbon (PSR-AC), Chemosphere, 86 (2012) 648-654.
[39] C.S. Kim, G.E. Brown Jr, J.J. Rytuba, Characterization and speciation of mercury-bearing mine wastes using X-ray absorption spectroscopy, Sci. Total Environ., 261 (2000) 157-168.
[40] B. Meng, X. Feng, G. Qiu, C.W.N. Anderson, J. Wang, L. Zhao, Localization and speciation of mercury in brown rice with implications for pan-Asian public health, Environ. Sci. Technol., 48 (2014) 7974-7981.
[41] L. Vincze, B. Vekemans, F.E. Brenker, G. Falkenberg, K. Rickers, A. Somogyi, M. Kersten, F. Adams, Three-dimensional trace element analysis by confocal X-ray microfluorescence imaging, Anal. Chem., 76 (2004) 6786-6791.
[42] S. Choudhury, J.K. Thomas, N.J. Sylvain, O. Ponomarenko, R.A. Gordon, S.M. Heald, D.M. Janz, P.H. Krone, I. Coulthard, G.N. George, I.J. Pickering, Selenium preferentially accumulates in the eye lens following embryonic exposure: A confocal x-ray fluorescence imaging study, Environ. Sci. Technol., 49 (2015) 2255-2261.
[43] D.W. Blowes, C.J. Ptacek, J.L. Jambor, In-situ remediation of Cr(VI)-contaminated groundwater using permeable reactive walls: Laboratory studies, Environ. Sci. Technol., 31 (1997) 3348-3357.
[44] US EPA, Method 1631: Revision E: Mercury in water by oxidation, purge and trap, and cold vapor atomic fluorescence spectrometry, in, Washington DC, USA, 2002.
[45] US EPA, 40 CFR Appendix B to Part 136 - Definition and procedure for the determination of the method detection limit-Revision 1.11, in, U.S. Environmental Protection Agency, Washington DC, USA, 2011.
[46] B. Ravel, M. Newville, ATHENA, ARTEMIS, HEPHAESTUS: Data analysis for X-ray absorption spectroscopy using IFEFFIT, J. Synchrotron Radiat., 12 (2005) 537-541.
[47] A.R. Woll, D. Agyeman-Budu, D.H. Bilderback, D. Dale, A.Y. Kazimirov, M. Pfeifer, T. Plautz, T. Szebenyi, G. Untracht, 3D X-ray fluorescence microscopy with 1.7 μm resolution using lithographically fabricated micro-channel arrays, in Advances in X-Ray/EUV Optics and Components VII, Proceedings of SPIE, (2012) 85020K.
[48] A.R. Woll, D. Agyeman-Budu, S. Choudhury, I. Coulthard, A.C. Finnefrock, R. Gordon, E. Hallin, J. Mass, Lithographically-fabricated channel arrays for confocal X-ray fluorescence microscopy and XAFS, J. Phys. Conf. Ser., 493 (2014) 012028.

[49] D.N. Agyeman-Budu, S. Choudhury, I. Coulthard, R. Gordon, E. Hallin, A.R. Woll, Germanium collimating micro-channel arrays for high resolution, high energy confocal X-ray fluorescence microscopy, in AIP Conference Proceedings, (2016) 020004-1–020004-11.
[50] P. Liu, C.J. Ptacek, D.W. Blowes, Y.Z. Finfrock, R.A. Gordon, Stabilization of mercury in sediment by using biochars under reducing conditions, J. Hazard. Mater., 325 (2017) 120-128.
[51] AMCSD American Mineralogist Crystal Structure Database. http://rruff.geo.arizona.edu/AMS/amcsd.php.
[52] The Atoms.inp archive. http://cars.uchicago.edu/~newville/adb/search.html.
[53] P. Liu, C.J. Ptacek, D.W. Blowes, W.R. Berti, R.C. Landis, Aqueous leaching of organic acids and dissolved organic carbon from various biochars prepared at different temperatures, J. Environ. Qual., 44 (2015) 684-695.
[54] U. Skyllberg, Competition among thiols and inorganic sulfides and polysulfides for Hg and MeHg in wetland soils and sediments under suboxic conditions: Illumination of controversies and implications for MeHg net production, J. Geophys. Res., 113 (2008) 1-14.
[55] C. Dezarnaud, M. Tronc, A.P. Hitchcock, Inner shell spectroscopy of the carbon-sulfur bond, Chem. Phys., 142 (1990) 455-462.
[56] Y. Dauphin, M. Salomé, Chemical mapping with X-ray absorption spectroscopy, in: E. DiMasi, L.B. Gower (Eds.) Biomineralization Sourcebook: Characterization of Biominerals and Biomimetic Materials, CRC Press, Taylor & Francis Group, Boca Raton, FL, USA, 2014, pp. 73-93.
[57] B.P. Singh, A.L. Cowie, R.J. Smernik, Biochar carbon stability in a clayey soil as a function of feedstock and pyrolysis temperature, Environ. Sci. Technol., 46 (2012) 11770-8.
[58] X. Xiao, B. Chen, A direct observation of the fine aromatic clusters and molecular structures of biochars, Environ. Sci. Technol., 51 (2017) 5473-5482.
[59] J. Sandström, I. Wennerbeck, Tautomeric cyclic thiones, Acta Chem. Scand., 20 (1966) 57-71.
[60] Z.V. Todres, Chalcogenadiazoles: Chemistry and Applications, CRC Press, Taylor & Francis Group, Boca Raton, FL, 2011.
[61] J. Zhu, B. Deng, J. Yang, D. Gang, Modifying activated carbon with hybrid ligands for enhancing aqueous mercury removal, Carbon, 47 (2009) 2014-2025.
[62] F. Aboufazeli, H.R.L.Z. Zhad, O. Sadeghi, M. Karimi, E. Najafi, Synthesis and characterization of novel poly-thiophene-nanoporous silica and its application for mercury removal from waste waters, J. Macromol. Sci., Pure Appl. Chem., 50 (2013) 18-24.
[63] T.M. Bisson, L.C.W. MacLean, Y. Hu, Z. Xu, Characterization of mercury binding onto a novel brominated biomass ash sorbent by X-ray absorption spectroscopy, Environ. Sci. Technol., 46 (2012) 12186-12193.
[64] E. Schuster, The behavior of mercury in the soil with special emphasis on complexation and adsorption processes-a review of the literature, Water Air Soil Poll., 56 (1991) 667-680.
[65] A. Walcarius, C. Delacôte, Mercury(II) binding to thiol-functionalized mesoporous silicas: critical effect of pH and sorbent properties on capacity and selectivity, Anal. Chim. Acta, 547 (2005) 3-13.

[66] P. Lessi, N.L. Dias Filho, J.C. Moreira, J.T.S. Campos, Sorption and preconcentration of metal ions on silica gel modified with 2,5-dimercapto-1,3,4-thiadiazole, Anal. Chim. Acta, 327 (1996) 183-190.
[67] W. Tang, D. Bruce Chase, D.L. Sparks, J.F. Rabolt, Selective and quantitative detection of trace amounts of mercury(II) ion (Hg^{2+}) and copper(II) ion (Cu^{2+}) using surface-enhanced raman scattering (SERS), Appl. Spectrosc., 69 (2015) 843-849.
[68] S.I. Hussain, D.W. Blowes, C.J. Ptacek, D. Olding, Phosphorus removal from lake water using basic oxygen furnace slag: System performance and characterization of reaction products, Environ. Eng. Sci., 31 (2014) 631-642.
[69] U.S. Environmental Protection Agency, *In-situ* chemical reduction at the Morses Pond Culvert, Wellesley, Massachusetts, 2001. https://frtr.gov/costperformance/profile.cfm?ID=351&CaseID=351
[70] S.W. Petersen, K.A. Hedquist, F. Hanford, Teatability test report for calcium polysulfide in the 100-K area, US Department of Energy, 2006.
[71] K.A. Spokas, Review of the stability of biochar in soils: Predictability of O:C molar ratios, Carbon Manag., 1 (2010) 289-303.